

## PEGylated nanostructured lipid carriers loaded with 10-hydroxycamptothecin: an efficient carrier with enhanced anti-tumour effects against lung cancer

Xinxin Zhang, Yong Gan, Li Gan, Shufang Nie and Weisan Pan

### Abstract

Most drugs do not have the pharmacokinetic features required for optimal pulmonary delivery. In this study, we developed PEGylated nanostructured lipid carriers (PEG-NLCs) to improve the delivery of anti-tumour agents to lung tumours. PEG-40 NLCs modified with PEG-40 stearate (molecular weight 2000 Da), PEG-100 NLCs modified with PEG-100 stearate (molecular weight 5000 Da) and NLCs without PEG modification were prepared by melt-emulsification and homogenization, and were loaded with 10-hydroxycamptothecin (HCPT). They were investigated in terms of physiological characteristics, biodistribution, cellular uptake, and anti-tumour effect in-vivo. PEG-NLCs exhibited regular morphology, with a spherical shape. The particle size (measured by laser diffraction) was approximately 100 nm. Encapsulation in PEG-NLCs protected the active lactone form of HCPT compared with HCPT solution after incubation with plasma. In biodistribution studies, PEG-NLCs, especially PEG-40 NLCs, had longer circulation time and decreased uptake by the reticuloendothelial system (RES) compared with unmodified NLCs. PEG-NLCs accumulated in the lungs after i.v. injection in mice. PEG-NLCs showed enhanced cellular uptake by human lung adenocarcinoma epithelial A549 cells. In-vivo experiments indicated that PEG-NLCs loaded with HCPT have superior efficacy against A549 lung cancer compared with HCPT solution and NLCs. These results suggest that PEG-NLCs is a promising delivery system for HCPT in the treatment of lung cancer.

### Introduction

Camptothecin (CPT) and its analogues are promising anti-tumour agents. They inhibit nuclear enzyme topoisomerase I (Jaxel et al 1989), which blocks DNA replication and thus selectively affects cancer cells. Studies in animal and human subjects have shown that 10-hydroxycamptothecin (HCPT) is more potent and less toxic than the parent compound CPT. HCPT has strong anti-tumour activity against a wide range of tumours (Zhou et al 1991), including hepatoma, gastric carcinoma, leukaemia, and head and neck tumours. However, there are obstacles to the wide clinical application of HCPT. First, because of the poor solubility in water and physiologically acceptable organic solvents, the development of HCPT dosage forms is limited. Moreover, the lactone form of HCPT exists in a pH-dependent equilibrium with an open carboxylate form (Figure 1). The lactone is the biologically active form whereas the carboxylate form may render the drug much less active and highly toxic (Igor et al 1998; O'Leary & Muggia 1998). The lactone opens rapidly to the carboxylate form even in human plasma. In addition, the anti-tumour activity of CPT is time dependent, and prolonged supply improves efficacy (Inaba 1994). The short half-life ( $t_{1/2}$ ; about 30 min) of HCPT means that frequent administration is required, and intensifies the side-effects of the drug.

HCPT currently approved for clinical use is a sodium salt solution of the carboxylate form, which has a  $t_{1/2}$  of only about 30 min. It has minimal anticancer activity and unpredictable side-effects such as myelosuppression, haemorrhagic cystitis, diarrhoea, nausea, vomiting and dermatitis (Wani et al 1980).

Attempts have been made to develop novel delivery systems to stabilize the lactone-formed CPTs or prolong plasma  $t_{1/2}$  of HCPT. Polymeric nanoparticles (Leyang et al 2007),

School of Pharmacy, Shenyang  
Pharmaceutical University, 103  
Wenhua Road, P.O. Box 122,  
Shenyang 110016, PR China

Xinxin Zhang, Shufang Nie,  
Weisan Pan

Shanghai Institute of Materia  
Medica, Shanghai Institutes  
for Biological Sciences, Chinese  
Academy of Science,  
555 Zu-Chong-Zhi Road,  
Shanghai 201203, PR China

Xinxin Zhang, Yong Gan, Li Gan

**Correspondence:** Weisan Pan,  
School of Pharmacy, Shenyang  
Pharmaceutical University, 103  
Wenhua Road, P.O. Box 122,  
Shenyang 110016, PR China.  
E-mail: xinxin\_8209@hotmail.com

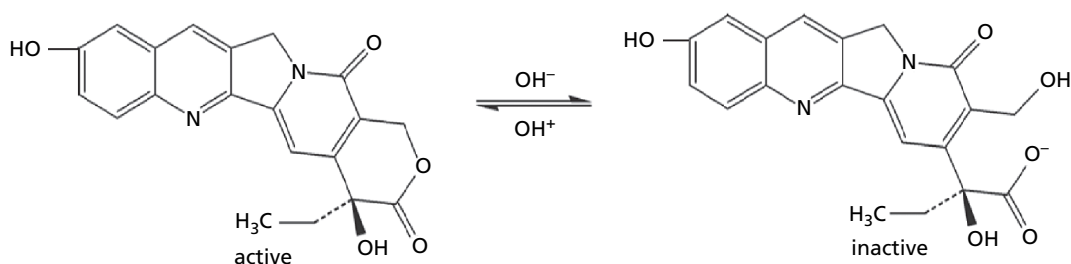


**Figure 1** The structure of hydroxycamptothecin (HCPT) and equilibrium reaction between the active form and inactive form.

liposomes (Cortesi et al 1997) and micelles (Zerrin et al 2006) have been explored with some success. A problem common to these new formulas is rapid uptake by the reticuloendothelial system (RES) and subsequent accumulation in the liver and spleen. This phenomenon reduces the effectiveness of HCPT for treating tumours and increases the toxicity to the RES. In addition, degradation of polymeric materials may cause potential toxicity on systemic administration (Alexander 2006). Thus, a new drug delivery system that avoids RES uptake and increases tumour/tissue targeting would be very useful to obtain a higher anti-tumour efficacy and decrease the side-effects of HCPT.

Nanostructured lipid carriers (NLCs) are an improved generation of lipid nanoparticles (Müller et al 2002) developed from solid lipid nanoparticles (SLNs). NLCs consist of solid lipid matrices with spatially incompatible liquid lipids. They retain many advantages of SLNs (e.g. controlled drug release, biocompatibility and the possibility of production on a large industrial scale) whilst also minimizing certain problems associated with SLNs (drug leakage during storage and limited drug loading capacity).

PEGylated nanoparticles have been reported to be less susceptible to uptake by the RES, with increased half-life in the circulation (Moghimi et al 2001). Furthermore, PEG can prolong exposure of tumour cells to nanoparticles loaded with an anti-tumour drug and enhance permeability and retention (EPR) effects (Maeda et al 2000).

In the present study, PEGylated NLCs (PEG-NLCs) were prepared as carriers to stabilize the lactone-form of HCPT, prolonging the circulation time of the drug and increasing its anti-tumour activity against lung cancer. PEG-NLCs were investigated in terms of physiological characteristics, stability of the HCPT lactone form in plasma, in-vitro release, biodistribution, cellular uptake and in-vivo anti-tumour effect. In this work, we found a novel lung-targeting effect of PEG-NLCs after i.v. injection in mice. PEG-NLCs showed increased uptake by human lung adenocarcinoma epithelial A549 cells, and produced a superior anti-tumour efficacy against the A549 lung cancer.

## Material and Methods

### Materials

HCPT was from the Shanghai Junjie Biotechnology Co., Ltd (China). Monostearin (Rikevita Co. Ltd, Tokyo, Japan) was

chosen as the solid lipid matrix of NLCs and purified soybean oil 788 (Lipoid GmbH, Ludwigshafen, Germany) was used as the liquid lipid for NLCs. Lecithin was from Lipoid Co. Pluronic F68 was a gift from BASF Co., Ltd (Ludwigshafen, Germany). Pyrene and polyethylene glycol stearates with polymerization degrees of 40 and 100 (PEG-40 stearate and PEG-100 stearate, respectively) were from Sigma-Aldrich (New York, USA). Other reagents were of analytical grade or higher.

### Animals and cell culture

Female KM mice and BALB/cA nu/nu mice ( $20 \pm 2$  g, 4–5 weeks of age) were bred at the Shanghai Institute of Materia Medica (Shanghai, China). Mice were housed in sterile cages within laminar airflow hoods in a specific pathogen-free room with a 12 h light–dark schedule. Food and water were autoclaved. All experiments were carried out according to institutional ethical guidelines on animal care and use. The human lung adenocarcinoma epithelial cell line A549 was from the Shanghai Institute of Materia Medica. Cells were cultured in F-12K medium (Gibco, New York, USA) supplemented with 10% fetal bovine serum (Gibco),  $100 \text{ U mL}^{-1}$  penicillin and  $100 \text{ U mL}^{-1}$  streptomycin. Cultures were maintained at  $37^\circ\text{C}$ , 5%  $\text{CO}_2$  and 100% humidity.

### Preparation of HCPT-loaded PEG-NLCs and NLCs without PEG modification

Compositions of the formulations used in this work, including HCPT-loaded PEG-NLCs and NLCs without PEG modification, are given in Table 1. PEG-NLCs were prepared using melt emulsification followed by high-pressure homogenization. Briefly, HCPT was dissolved in lecithin. Monostearin and soybean oil were then added and the mixture was melted at  $80^\circ\text{C}$ . The hot oil phase was dispersed in an aqueous solution containing PEG stearate of the same temperature, and a coarse emulsion was formed using an Ultra Turrax (IKA, Guangzhou, China) at  $6500 \text{ rev min}^{-1}$  for 10 min. The hot coarse emulsion was then homogenized under 800 bar at  $60^\circ\text{C}$  with a high-pressure homogenizer (NS1001L, GEA, Sala Baganza, PR, Italy) for eight cycles. The dispersions were subsequently allowed to recrystallize at room temperature. PEG-NLCs prepared using PEG-40 stearate and PEG-100 stearate (PEG molecular weights: 2000 and 5000 Da) are designated as PEG-40 NLCs and PEG-100 NLCs, respectively. HCPT-loaded NLCs (without PEG modification) were

**Table 1** Composition, particle size, polydispersity index, entrapment efficiency and zeta potential of the developed HCPT-loaded PEG-NLCs and NLCs (without PEG modification). PEG-40 NLCs 2 were used for all subsequent experiments

	PEG-40 NLCs <sup>a</sup>				PEG-100 NLCs	NLCs
	1	2	3	4		
<b>Composition (% w/w)</b>						
HCPT	0.05	<b>0.05</b>	0.05	0.05	0.05	0.05
Monostearin	4.5	<b>4.0</b>	3.5	3.0	4.0	4.0
Soybean oil	0.5	<b>1.0</b>	1.5	2.0	1.0	1.0
Lecithin	1.5	<b>1.5</b>	1.5	1.5	1.5	1.5
PEG-40 stearate	1.8	<b>1.8</b>	1.8	1.8	–	–
PEG-100 stearate	–	–	–	–	1.8	–
Pluronic F68	–	–	–	–	–	1.0
Water q.s.	100	<b>100</b>	100	100	100	100
<b>Characteristic</b>						
Particle size (nm)	102.9 ± 7.1	<b>88.6 ± 2.5</b>	90.9 ± 2.8	85.3 ± 4.3	101.5 ± 3.2	91.5 ± 4.5
Polydispersity index	0.186 ± 0.025	<b>0.065 ± 0.021*</b>	0.174 ± 0.029	0.304 ± 0.033	0.106 ± 0.018	0.114 ± 0.020
Entrapment efficiency (%)	88.8 ± 1.1	<b>92.2 ± 1.8*</b>	85.7 ± 0.9	81.6 ± 2.5	90.8 ± 1.2	88.6 ± 2.3
Zeta potential (mV)	–10.29 ± 0.31	<b>–10.62 ± 0.65</b>	–10.97 ± 0.28	–11.51 ± 0.47	–10.71 ± 0.52	–32.53 ± 0.43

<sup>a</sup>PEG-40 NLCs 1–4 had solid:liquid lipid ratios of 9:1, 8:2, 7:3 and 6:4, respectively.

Data are mean ± s.d. (n = 3).

\**P* < 0.05.

prepared in the same manner as PEG-NLCs, but PEG stearate was replaced by Pluronic F68.

## Characterization

### Particle size, zeta potential and morphology

Particle size, size distribution and zeta potential of PEG-NLCs and NLCs were determined using a laser diffraction particle size analyser (Nicomp 380 ZLS zeta potential/particle sizer, Santa Barbara, CA, USA). Samples were diluted with double-distilled water to an adequate scattering intensity prior to the measurement. Morphology of PEG-NLCs was examined using a JEM-1230 transmission electron microscope (TEM; JEOL, Tokyo, Japan). PEG40-NLCs and PEG100-NLCs were dispersed in distilled water and stained with 2% phosphotungstic acid, and then placed on copper grids with film for viewing.

### Drug entrapment efficiency determination

Free HCPT (not incorporated in the carriers) was separated using an ultrafiltration–centrifugation technique (Michalowski et al 2004). A 500 µL sample of HCPT-loaded PEG-NLCs/NLCs was placed into Microcon YM-10 filter units (10000 MW, Millipore, CT, USA) and centrifuged at 4000 revmin<sup>–1</sup> for 10 min. The total HCPT concentration in PEG-NLCs / NLCs was measured using HPLC after dissolving the samples in methanol. Free HCPT not incorporated into the PEG-NLCs/NLCs was measured in the separated ultrafiltrate. The % entrapment efficiency (EE) was calculated according to the following equation:  $EE = ([W_T - W_F] / W_T) \times 100\%$ , where  $W_T$  is the weight of total drug in PEG-NLCs/NLCs and  $W_F$  is the weight of free drug in the ultrafiltrate after centrifugation.

### Determination of fixed aqueous layer thickness (FALT) and PEG density

FALT of PEG-40 NLCs and PEG-100 NLCs was calculated using the Gouy–Chapmann theory (Yasuyuki et al 2002). According to this theory, zeta potential  $\psi$  (L) as the electrostatic potential at the position of the slipping plane L (nm) is expressed as:  $\ln \psi(L) = \ln A - \kappa L = \sqrt{C}/0.3$ , where A is a constant,  $\kappa$  is the Debye–Hückel parameter (i.e.  $\sqrt{C}/0.3$ ) and C is the molarity of electrolytes for univalent salt. If zeta potentials are measured in various concentrations of NaCl and plotted against  $\kappa$ , the slope L gives the position of the slipping plane or thickness of the fixed aqueous layer in nm (Shimada et al 1995; Sadzuka & Hirota 1997).

PEG concentration was measured using a colorimetric method (Sims & Snape 1980). Practically, standards (PEG 0–20 µg mL<sup>–1</sup>) or PEG-NLCs samples were added to 10 mL water and mixed with 250 µL of a reagent consisting of I<sub>2</sub> (10 g L<sup>–1</sup>) and KI (20 g L<sup>–1</sup>). Absorbance was measured at 525 nm. The surface density of the PEG chains (1/S) was calculated according to the following equation (Peracchia et al 1997):  $1/S = N_{PEG} / Snp = N d \alpha r / 3MW_{PEG}$ , where  $N_{PEG}$  is the total number of PEG chains,  $\alpha$  is the PEG content at the surface of the NLCs (% of the PEG-NLCs weight), Snp is the surface area of the nanoparticles, and N, d, r,  $MW_{PEG}$  represent Avogadro's number, density of PEG-NLCs, particle size and PEG molecular weight, respectively.

The average distance D between two neighbouring PEG chains was derived from the surface density of PEG chains:  $D = \sqrt{S}$

### In-vitro release study

Release of HCPT from PEG-NLCs was examined in phosphate buffered saline (pH 7.4; PBS) using a dialysis method.

A 6 mL sample of PEG-NLCs was placed in the dialysis bag with a cut-off molecular weight of 12–14 kDa. The bags were immersed in 500 mL PBS at 37°C. The paddle rotation speed was 50 revmin<sup>-1</sup>. At selected time intervals, 8 mL dialysis buffer was taken out for analysis and replaced with the same volume of fresh medium. Samples were acidified with glacial acetic acid (50 µL) prior to analysis by HPLC.

### Stability of HCPT lactone form in plasma

One millilitre samples of HCPT-loaded PEG-40 NLCs, PEG-100 NLCs and HCPT solution (sodium salt) were added to 10 mL plasma, and stirred with a magnetic bar at 37°C. Samples (200 µL) of the mixture were then taken at selected time intervals and transferred to polypropylene vials containing 200 µL ice-cold methanol, vortex mixed (5 min) and centrifuged (10000 rpm for 10 min). The concentration of the HCPT lactone form in the methanol extract was determined using HPLC.

### Pharmacokinetics and biodistribution in mice

KM mice (20 ± 2 g) were used for biodistribution studies. Mice were fasted overnight but had free access to water. Preparations were injected i.v. via the tail vein. For each preparation and each sampling time point, three mice were treated with a single dose of HCPT of 2.5 mgkg<sup>-1</sup> given as HCPT solution (sodium salt), HCPT-loaded NLCs, PEG-40 NLCs or PEG-100 NLCs.

Blood samples were collected at predetermined times into heparinized test tubes from the ocular artery after eyeball removal, and centrifuged immediately to obtain plasma. Organs were then removed and samples were weighed, homogenized with saline and acidified to pH 3.0 with phosphoric acid.

### HPLC analysis of HCPT

The internal standard (100 µL CPT) and 3 mL ethyl acetate were added to 0.5 mL plasma/tissue sample and extracted for 5 min. The mixture was centrifuged at 5000 revmin<sup>-1</sup> for 10 min, then 2.5 mL of the supernatant was dried under nitrogen and dissolved in 200 µL mobile phase. The solution was centrifuged at 8000 revmin<sup>-1</sup> for 15 min before HPLC analysis.

The concentration of the HCPT lactone form was measured using reverse-phase HPLC with an LC-20A system (Shimadzu, Kyoto, Japan). Analysis was done using a Zorbax SB-C18 5 µm, 150 × 4.6 mm column (Agilent, CA, USA). The mobile phase consisted of a 50:50 mixture of aqueous triethylamine-acetate buffer (pH 6.0) and methanol, and was delivered at a flow rate of 1.0 mLmin<sup>-1</sup>. HCPT was monitored at 382 nm.

### Uptake by A549 cells

A549 cells were seeded into 24-well plates at a density of 10000 cells per well and cultured in 1 mL F-12K at 37°C. PEG-NLCs (50 µL) or NLCs labelled with 0.02% pyrene was added to each well. After predefined periods of incubation, the supernatants were removed. Cells were washed three times with PBS and examined using an inverted fluorescence microscope (IX71, Olympus, Tokyo, Japan). The amount of

label associated with the cells was assayed by dissolving cells in DMF and analysed by fluorospectrophotometry (λ excitation 375 nm, λ emission 402 nm). The number of cells that had taken up the fluorescence marker was counted.

### Anti-tumour effects in mice bearing A549 lung cancer

A549 cells (5 × 10<sup>6</sup> cells per mouse) were inoculated subcutaneously into the axillary region of BALB/cA nu/nu mice (20 ± 2 g). When the tumours reached an average volume of 100–200 mm<sup>3</sup>, mice were randomly grouped (six per group) to receive an injection (2.5 mgkg<sup>-1</sup>) of HCPT solution (sodium salt), HCPT-loaded NLCs, PEG-40 NLCs, PEG-100 NLCs or saline via the tail vein twice a week for 3 weeks. Tumours were measured twice a week using microcallipers. The tumour volume (V) was calculated as follows:  $V = (\text{length} \times \text{width}^2)/2$ . The relative tumour volume (RTV) was used as an index of anti-tumour activity, and calculated as follows:  $RTV = V_t/V_0$ , where  $V_t$  and  $V_0$  are the volumes before and after treatment, respectively.

### Statistical analysis

Statistical analysis of the effect of lipid matrix compositions (ratios between solid lipid and liquid lipid 9:1, 8:2, 7:3 and 6:4) on the particle size distribution and entrapment efficiency of PEG-40 NLCs was performed using one-way analysis of variance. The effect of formulation on the stability of the HCPT lactone form, pharmacokinetics, biodistribution and in-vivo anti-tumour effects was evaluated by the Student's *t*-test. Data are presented as mean ± s.d. Differences were considered significant when *P* was less than 0.05.

## Results and Discussion

### Characteristics of PEG-NLCs and NLCs

Table 1 showed the particle size, size distribution, zeta potential and entrapment efficiency of HCPT-loaded PEG-NLCs and NLCs (without PEG modification). The particles of the developed formulations, including HCPT-loaded PEG-NLCs and NLCs, were about 100 nm diameter, and polydispersity index (PI) values for all formulations were relatively low (<0.3). The entrapment efficiency of HCPT in PEG-NLCs and NLCs was more than 80%. The particle size distribution and entrapment efficiency of PEG-NLCs were related to the ratio of solid lipid to liquid lipid. To investigate the influence of lipid-phase composition, PEG-NLCs composed of 5% lipid phase at different ratios of solid lipid to liquid lipid were prepared (i.e. 9:1, 8:2, 7:3 and 6:4; Table 1). For instance, PEG-40 NLCs had similar particle size (~100 nm) when prepared with different ratios of solid lipid to liquid lipid. PEG-40 NLCs 2 (ratio of 8:2) showed significantly narrow distribution (PI=0.065) and high entrapment efficiency (92.2%) compared with other formulations of PEG-40 NLCs (*P*<0.05). When the content of liquid lipid (soybean oil) was below or exceeded 20%, PEG-40 NLCs had a broader

distribution and lower entrapment efficiencies. A similar trend was seen with PEG-100 NLCs (data not shown).

The influence of lipid-phase composition on PI and entrapment efficiency could be explained as follows: when the proportion of liquid lipid in the lipid matrix was less than 20% (PEG-40 NLCs 1), this was insufficient to embed every nanoparticle formed by solid lipids. A few nanoparticle crystals composed of solid lipids without embedded liquid lipids will therefore emerge in the system. This high-ordered crystal induces drug expulsion and reduces entrapment efficiency (Müller et al 2002). The different crystal forms of the nanoparticles lead to large PI. Liquid lipid in excess of 20% (PEG-40 NLCs 3 and 4), was too high to be loaded within the solid lipid matrix of NLCs. Separate oil droplets would therefore exist in the system, and lead to a relative wide distribution and low entrapment efficiency. Based on the experiments above, we chose PEG-40 NLCs 2 (20% soybean oil in lipid matrix) for further studies.

Surface charge is important in nanoparticle systems. In general, higher surface charge of the nanoparticles leads to stronger repulsion interactions among nanoparticles in dispersion, and hence higher stability. The zeta potential of PEG-40 NLCs and PEG-100 NLCs was about  $-10$  mV. NLCs without PEG surface coating had a more negative zeta potential (about  $-33$  mV; Table 1). These findings are consistent with a previous report showing that the PEG outer-shell reduces the surface charge (Hawley et al 1997). Despite reduced charge, PEG-NLCs were stable, probably because of stereospecific blockade between nanoparticles.

The TEM images in Figure 2 show that PEG-40 NLCs and PEG-100 NLCs were spherical, with a particle size of approximately 100 nm.

Interaction of the PEG polymer with the surrounding water molecules results in a fixed aqueous layer around the NLCs. This water-gathered surface prevents the attachment of opsonins (Yasuyuki et al 2002). The approaching protein compresses the PEG chains and induces steric repulsion (Peracchia et al 1997). Thus, it was critical to determine the

FALT, in order to predict the long-circulation  $t_{1/2}$  of nanoparticles. In this study, FALT was proportional to the molecular weight of PEG stearate (Table 2). However, larger FALT or longer PEG chains do not necessarily lead to greater reductions in RES uptake. The ability to avoid uptake also depends on the PEG density and on the distance between adjacent PEG chains of PEG-NLCs. According to a model for the repulsion of protein from solid surfaces of MePEG<sub>2000</sub>-PLA nanoparticles (Jeon et al 1991; Jeon & Andrade 1991), phagocytosis occurs if the density of PEG chains is beyond the range of  $1.5\text{--}2\text{ nm}^2$  per PEG molecule (corresponding to a distance of  $1.2\text{--}1.4$  nm between two grafted PEG chains) (Bazile et al 1995). As Table 2 shows, the PEG density of PEG-40 NLCs was  $0.61\text{ nm}^2$  per PEG, compatible with a carrier with a long circulation  $t_{1/2}$  according to Jeon's model. The grafting density of PEG-100 NLCs was  $2.68\text{ nm}^2$  per PEG (distance between two PEG chains of  $1.64$  nm), which would result in phagocytosis according to the model.

### In-vitro release study

In order to evaluate the controlled release of the formulations, HCPT release from PEG-NLCs in-vitro over 48 h was investigated. Release curves, shown in Figure 3, indicate that release of HCPT from PEG-40 NLCs and PEG-100 NLCs was sustained, without an initial burst release. With the same particle size, the release rate of HCPT from PEG-NLCs depended on the molecular weight of PEG stearate. Longer PEG chains resulted in slower release of HCPT ( $56.5\%$  and  $43.3\%$  at 24 h for PEG-40 NLCs and PEG-100 NLCs, respectively). This is probably because the releasing mechanism of PEG-NLCs combines the effects of bulk erosion and diffusion. With increasing PEG molecular weight, FALT becomes larger, thus increasing the thickness of the diffusion layer. The results also suggest that encapsulation of HCPT in PEG-NLCs changed the drug release behaviour, and subsequently the carrier would affect the biodistribution in-vivo compared with free HCPT. The study of drug release in-vitro was

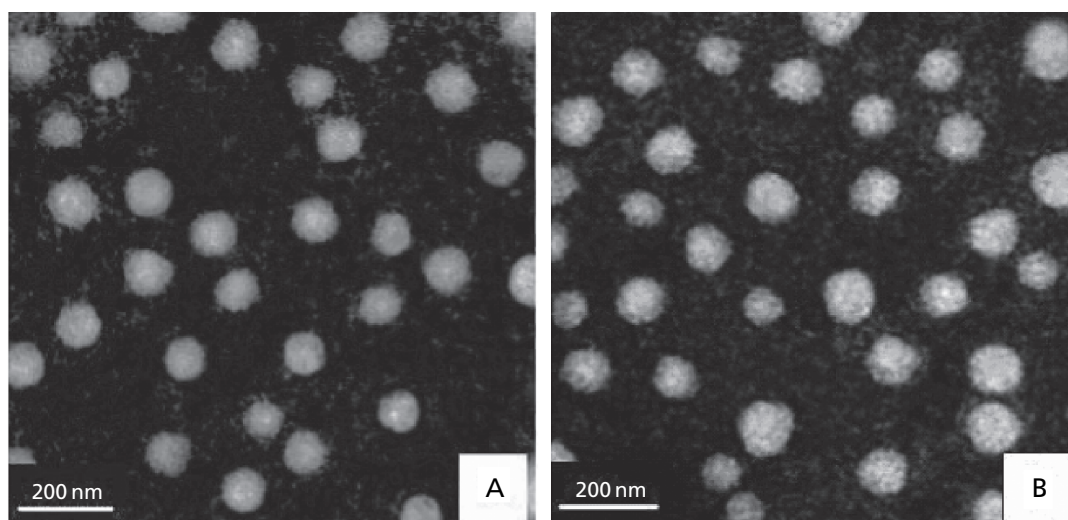


**Figure 2** Transmission electron microscope images of PEG-40 NLCs (A) and PEG-100 NLCs (B).

**Table 2** Fixed aqueous layer thickness (FALT), PEG density (surface area occupied by each PEG chain; S) and distance between two neighbouring PEG chains (D) of PEG-40 and PEG-100 NLCs

Sample	FALT (nm)	S (nm <sup>2</sup> per PEG)	D (nm)
PEG-40 NLCs	2.01 ± 0.07	0.61 ± 0.01	0.78 ± 0.02
PEG-100 NLCs	4.81 ± 0.11	2.68 ± 0.05	1.64 ± 0.03

Data are mean ± s.d. (n = 3).

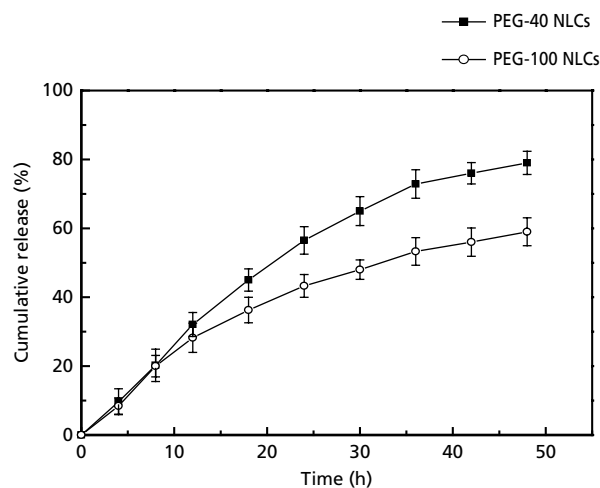


**Figure 3** Release profile of HCPT from PEG-40 NLCs and PEG-100 NLCs. Data are mean ± s.d. (n = 3).

performed without plasma or protein. The data only stands for the processes of HCPT dissolution and PEG-NLCs erosion in artificial body fluid. PEG-NLCs uptake and physiological disposition are more complicated in-vivo because of the effects of the immune system. Therefore, PEG molecular weight cannot be considered to be the most essential influencing factor in the behaviour of PEG-NLCs in-vivo; it needs to be characterized from a variety of PEG chain characters (e.g. PEG density and distance between PEG chains). The long-circulation  $t_{1/2}$  of the carrier should be demonstrated by pharmacokinetic and biodistribution studies.

### Stability of the HCPT lactone form in plasma

To check whether PEG-NLCs can protect the lactone form of HCPT, PEG-NLCs and HCPT solution were added to plasma to simulate physiological condition in-vivo. Consistent with the results obtained from clinical trials (Wani et al 1980), only about 10% of the lactone form of HCPT existed in plasma with the HCPT solution, regardless of the sampling time (Figure 4). This low proportion of the lactone form leads to poor therapeutic effect and systemic toxicity. Figure 4 shows that PEG-NLCs stabilized the HCPT lactone form. The concentration of the HCPT lactone form in plasma samples containing PEG-NLCs was significantly higher than in plasma samples containing the same amount of HCPT solution

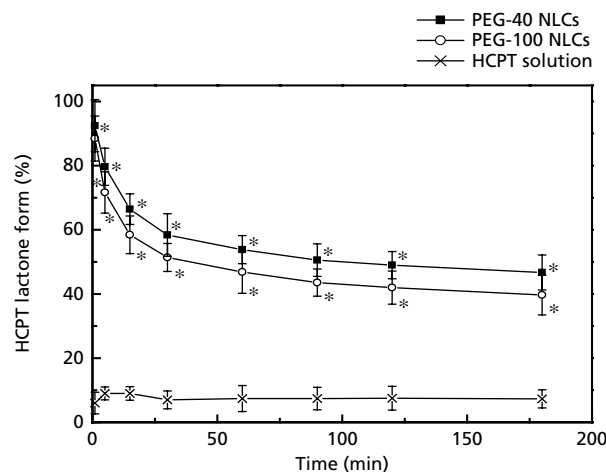


**Figure 4** Percentage of HCPT in the lactone form in PEG-40 NLCs, PEG-100 NLCs and solution in rat plasma at 37°C. Data are mean ± s.d. (n = 3). \* $P < 0.01$  vs HCPT solution.

( $P < 0.01$ ). Approximately 50% HCPT remained in lactone form in PEG-NLCs after 3 h incubation in plasma. Thus, encapsulation of HCPT in the lipid core of PEG-NLCs protected the lactone form from the effects of environmental pH. Similar effects were reported in lipidic nanoparticles for CPTs (Williams et al 2003). The percentage of lactone HCPT in PEG-40 NLCs and PEG-100 NLCs decreased rapidly within 1 h. We believe this is because some drug was dissolved in the emulsifier interfacial film and was more readily influenced by environmental pH due to plasma proteins. Because of the high binding of HCPT to plasma proteins (65–99%) and preferential binding of the carboxylate form (Mi & Burke 1994), plasma protein binding of the carboxylate will shift the equilibrium from the closed lactone form to the open carboxylate form (Figure 1). In comparison with PEG-40 NLCs, the larger distances between the PEG chains of PEG-100 NLCs (1.64 nm) cannot effectively prevent the approach of proteins (small plasma proteins can pass through the gap between PEG chains and touch the lipid core of NLCs) (Peracchia et al 1997). Therefore, the lactone ring of HCPT opens more quickly in PEG-100 NLCs than in PEG-40 NLCs, resulting in lower percentage of the lactone form.

### Pharmacokinetics and biodistribution in mice

Plasma levels of the different formulations were studied to determine the drug release profile in-vivo. The plasma HCPT concentration profiles after single i.v. injections of NLCs, PEG-40 NLCs, PEG-100 NLCs or HCPT solution at a dose of 2.5 mg kg<sup>-1</sup> are shown in Figure 5. Following injection, HCPT disappeared from circulation within 2 h, a reflection of its short  $t_{1/2}$ . By contrast, HCPT-loaded NLCs (without PEG modification) and PEG-NLCs showed a longer circulation time than the HCPT solution. The plasma HCPT concentration was much higher with PEG-NLCs than with HCPT solution or NLCs at each sampling time ( $P < 0.01$  versus NLCs).

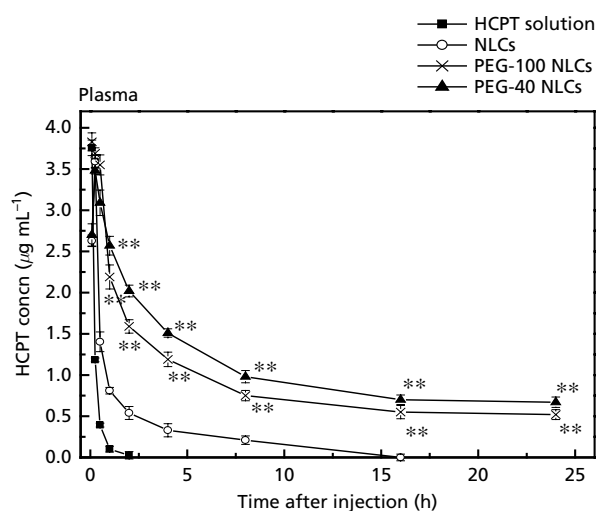


**Figure 5** Plasma concentration–time curves of HCPT after a single i.v.  $2.5 \text{ mg kg}^{-1}$  injection of HCPT solution, HCPT-loaded NLCs and PEG-NLCs to mice. Data are mean  $\pm$  s.d. ( $n=3$ ).  $**P < 0.01$ . Pharmacokinetic parameters of HCPT in plasma and lung after i.v. injection of HCPT solution, HCPT-loaded NLCs, PEG-40 NLCs and PEG-100 NLCs are listed in Table 3.

Pharmacokinetic parameters are summarized in Table 3. PEG-NLCs significantly increased the  $t_{1/2}$  (6.83 and 7.35 h) and resulted in larger areas under the plasma–concentration time curves ( $\text{AUC}_{0-24\text{h}}$   $20.94$  and  $25.85 \text{ } \mu\text{g h mL}^{-1}$ ) for HCPT compared with NLCs ( $t_{1/2}$ : 3.32;  $\text{AUC}_{0-24\text{h}}$ :  $5.17$ ) and HCPT solution ( $t_{1/2}$ : 0.47;  $\text{AUC}_{0-24\text{h}}$ :  $1.23$ ). It is logical that HCPT encapsulated in NLCs is released slowly and therefore shows sustained release after i.v. injection (Hu et al 2005). PEG-NLCs undergo minimal phagocytosis by the RES and thus remain in the circulation for a longer period of time than HCPT solution or NLCs.

To evaluate the distribution of PEG-NLCs in-vivo, HCPT concentrations in the tissues were measured after i.v. injection of HCPT solution, HCPT-loaded NLCs and PEG-NLCs. The distribution of HCPT in the liver, spleen, lungs, heart and kidneys is shown in Figure 6. It can be clearly seen that the biodistribution of HCPT was notably different in the groups

treated with NLCs or PEG-NLCs compared with HCPT solution. As expected, NLCs were distributed mainly to the RES organs (liver and spleen), with the majority accumulating in the liver. HCPT concentrations in the liver and spleen were significantly lower with PEG-NLCs than with NLCs (Figure 6A,C;  $P < 0.01$ ). PEG modification reduced uptake of nanoparticles by the RES. Significantly, the HCPT concentration in the liver and spleen was higher at most sampling times with PEG-100 NLCs than with PEG-40 NLCs. This distinction could be attributed to less optimal PEG density of PEG-100 NLCs (Table 2). The larger distance (1.64 nm) between PEG chains in PEG-100 NLCs facilitates protein access to the nanoparticles and initiates phagocytosis (Peracchia et al 1997). As shown in Figure 6D, the HCPT concentration in the kidneys was significantly lower with PEG-NLCs than with HCPT solution. Since renal toxicity is dose-limiting for CPTs (O'Reilly et al 1996), frequent administration of HCPT solution will intensify kidney injury. The results therefore indicate that PEG-NLCs are valuable for decreasing the renal toxicity of HCPT.

PEG-NLCs, and PEG-40 NLCs in particular, greatly increased the HCPT concentration in the lung (Figure 7E). The maximum concentration ( $C_{\text{max}}$ ) of HCPT in the lung was 40-fold higher with PEG-40 NLCs than with HCPT solution:  $\text{AUC}_{0-24\text{h}}$  was 14.51-fold greater and  $t_{1/2}$  increased by 4.55 fold (Table 3). NLCs and PEG-100 NLCs also resulted in higher HCPT concentration in the lung for a longer period of time. However, because of uptake by the RES, HCPT concentration in lung was significantly lower than with PEG-40 NLCs ( $P < 0.01$ ).

HCPT does not have the pharmacokinetic features required for optimal pulmonary delivery following i.v. injection.  $C_{\text{max}}$  in the lung for HCPT solution is only  $0.99 \text{ } \mu\text{g g}^{-1}$  tissue. Nanocarriers can optimize the pharmacokinetic properties of HCPT and improve drug delivery to the lung. Carrier size is one of the factors that affect drug distribution, circulation and cellular localization. Microspheres larger than  $10 \text{ } \mu\text{m}$  will embolize in the pulmonary capillary bed and create a high local concentration of drug. However, this aggregate of carrier will result in ischaemic vascular pockets, losing contact with the blood flow and nutrient exchange (Dziubla & Muzukantov 2006). Particles of  $0.5\text{--}1 \text{ } \mu\text{m}$  are capable of circulating in pulmonary capillaries, but they are unlikely to

**Table 3** Pharmacokinetic parameters of HCPT following single i.v. injection of HCPT ( $25 \text{ mg kg}^{-1}$ ) or nanoparticles to mice

	$\text{AUC}_{0-24\text{h}}$ ( $\mu\text{g h mL}^{-1}$ )	MRT (h)	$t_{1/2}$ (h)	CL ( $\text{mL h}^{-1}$ )	F
<b>Plasma</b>					
HCPT solution	$1.23 \pm 0.11$	$0.42 \pm 0.04$	$0.47 \pm 0.08$	$2.04 \pm 0.18$	–
NLCs	$5.17 \pm 0.63$	$2.96 \pm 0.36$	$3.32 \pm 0.09$	$0.45 \pm 0.06$	$4.20 \pm 0.14$
PEG-40 NLCs	$25.85 \pm 2.07$	$18.81 \pm 1.51$	$7.35 \pm 0.11$	$0.09 \pm 0.01$	$21.03 \pm 0.20$
PEG-100 NLCs	$20.94 \pm 2.10$	$20.56 \pm 0.18$	$6.83 \pm 0.12$	$0.13 \pm 0.01$	$17.01 \pm 0.19$
<b>Lung</b>					
HCPT solution	$3.06 \pm 0.21$	$3.30 \pm 0.23$	$4.92 \pm 0.09$	$0.36 \pm 0.02$	–
NLCs	$14.17 \pm 1.32$	$5.74 \pm 0.53$	$20.68 \pm 0.34$	$0.07 \pm 0.01$	$4.63 \pm 0.11$
PEG-40 NLCs	$44.40 \pm 3.29$	$7.14 \pm 0.53$	$22.38 \pm 0.27$	$0.04 \pm 0.01$	$14.51 \pm 0.08$
PEG-100 NLCs	$26.49 \pm 2.87$	$5.28 \pm 0.57$	$19.42 \pm 0.38$	$0.09 \pm 0.01$	$8.64 \pm 0.35$

AUC, area under the plasma–concentration time curve; MRT, mean residence time;  $t_{1/2}$ , plasma half-life; CL, clearance.

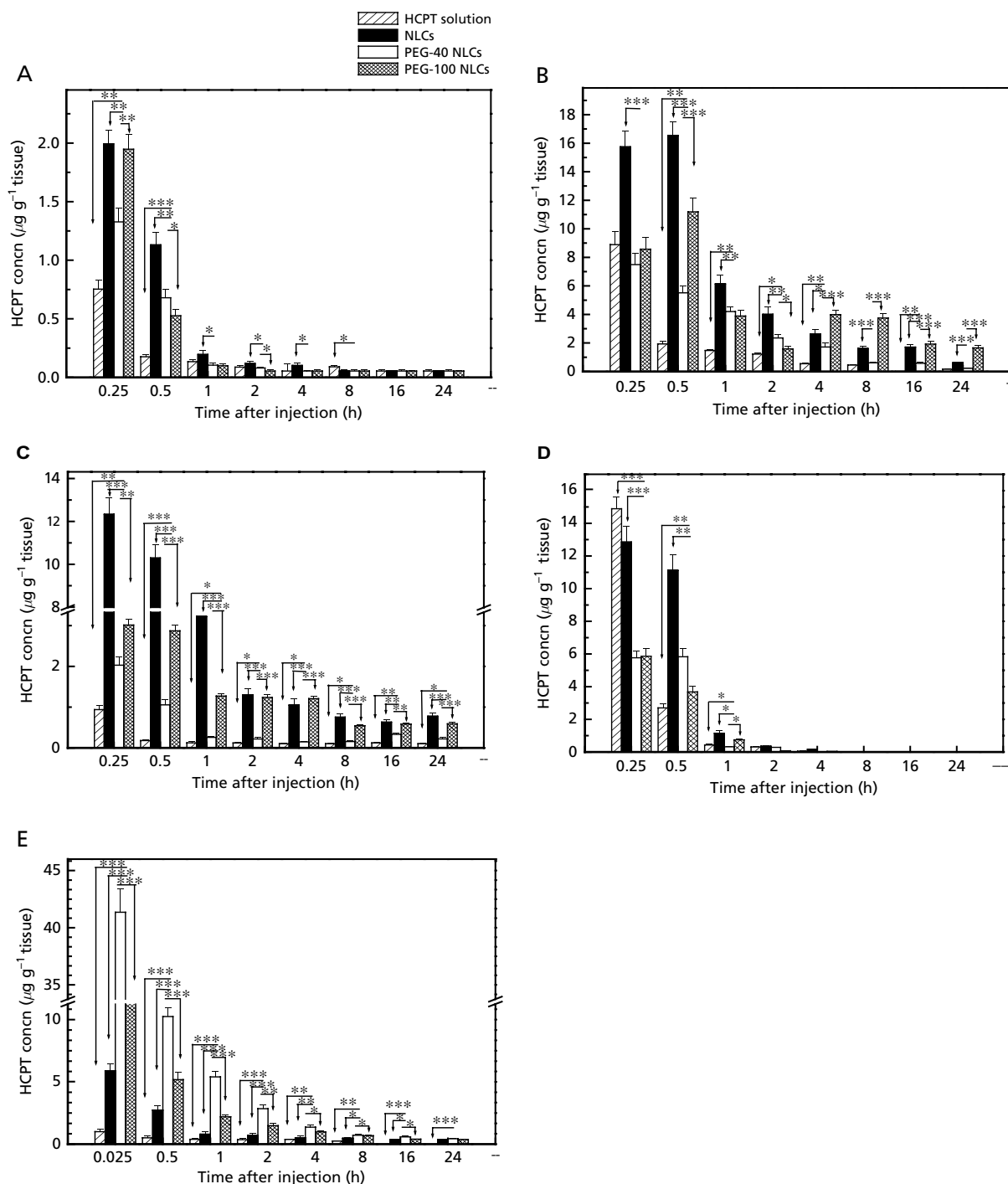


**Figure 6** Tissue distribution of HCPT to heart (A), liver (B), spleen (C), kidney (D) and lung (E) after a single 2.5 mg kg<sup>-1</sup> i.v. injection of HCPT solution, HCPT-loaded NLCs and PEG-NLCs to mice. Data are mean ± s.d. (n = 3 mice). \*P < 0.05; \*\*P < 0.01; \*\*\*P < 0.001. Pharmacokinetic parameters of HCPT in plasma and lung after i.v. injection of HCPT solution, HCPT-loaded NLCs, PEG-40 NLCs and PEG-100 NLCs are listed in Table 3.

leave the vascular lumen, and show inferior capacity to target the lungs. Nanocarriers about 100 nm in diameter are able to pass through the vascular endothelium and reach pulmonary alveoli. Therefore, PEG-NLCs of about 100 nm diameter show most potential for targeting the lungs. The pulmonary

targeting effect is also related to the physiological structure and function of the lungs. In order to cope with periods of high cardiac output and satisfy oxygen demands, blood pressure and the rate of perfusion in the lungs are significantly lower than in the systemic vasculature (Dziubla &

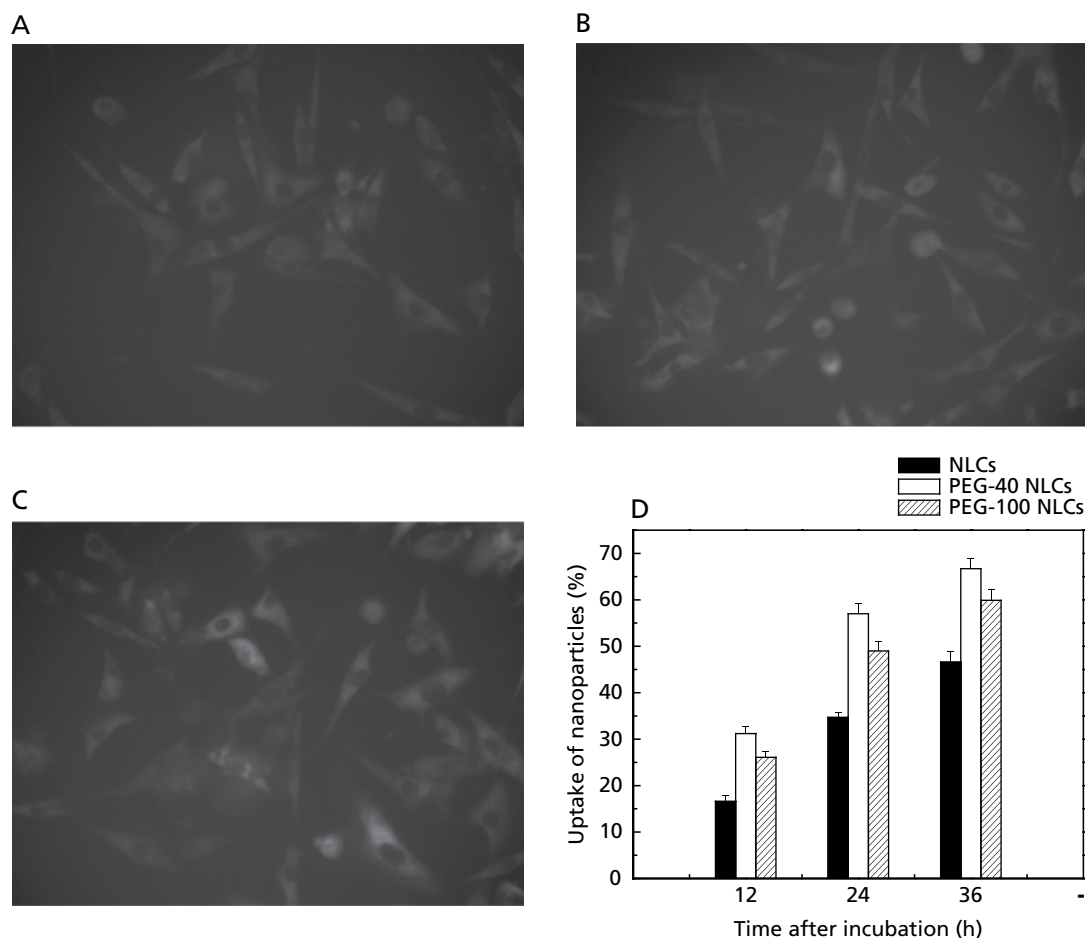


**Figure 7** Fluorescence microscopy images of the uptake of pyrene-labelled PEG-NLCs and NLCs by A549 cells. Cells were incubated for 24 h with NLCs (A), PEG-40 NLCs (B) or PEG-100 NLCs (C). Magnification  $\times 400$ . The uptake efficiencies for different nanoparticles by the A549 cells are shown in (D). Data are mean  $\pm$  s.d. ( $n = 3$ ).

Muzukantov 2006). This lays the foundation for the lung to receive high doses of injected drugs. Another mechanism that has been found to increase lung delivery is the EPR effect (Maeda et al 2003). The EPR effect was originally described when long-circulating stealth nanoparticles were shown to accumulate in vascularized solid tumours, a reflection of the erratic and highly permeable nature of the tumour vasculature. The vasculature of the lungs is also highly permeable, since the vascular bed receives the entire venous blood flow. It is plausible that EPR-related accumulation in the lung might occur. Indeed, reports have indicated that the pulmonary accumulation of nanoparticles is caused by the selective absorption by pneumocytes (Qingyu et al 2007). The alveolar epithelium is formed by type I and type II pneumocytes. The phospholipids and other pulmonary surfactants are synthesized and secreted by type II pneumocytes to degrade alveolar surface tension. The surfactant can be transported and suffers pinocytosis by type I pneumocytes (Serrano & Perez-Gil 2006). The addition of surface activity substances in PEG-NLCs, such as PEG stearate and phospholipid, could stimulate the adsorption of type I pneumocytes, and target PEG-NLCs to

the lungs. This enhanced lung uptake effect of PEG-NLCs shows promise for improving the therapeutic effect of HCPT in the treatment of lung cancer.

#### Uptake by A549 lung carcinoma cells

It is clear that the efficiency of cellular uptake of drug-loaded nanoparticles affects the therapeutic effects of the drug. Particles labelled with fluorescent dyes are frequently used to study cellular uptake. Some researchers had demonstrated that less than 0.6% of the incorporated dye could leach out from the nanoparticles over 48 h under in-vitro sink conditions (Desai et al 1997). Pyrene is a suitable marker for studying the cellular uptake of nanoparticles (Evangelos et al 2007). Pyrene was incorporated into PEG-NLCs and NLCs, and the efficiency of cellular uptake monitored by fluorescence microscopy. Figures 7A–C show the microscopic images of A549 cells after 24 h incubation with pyrene-labelled NLCs, PEG-40 NLCs and PEG-100 NLCs, respectively. It is evident that more PEG-NLCs were engulfed by A549 cells than NLCs after 24 h incubation. It can be seen that pyrene-labelled

NLCs and PEG-NLCs (blue) have been taken up by the cells, but they cannot enter the nuclei. Figure 7D shows the cellular uptake for all the samples during 36 h incubation. Obviously, more nanoparticles were taken up by A549 cells because of the extended exposure time. Cellular uptake was highest with PEG-40 NLCs and lowest with NLCs.

According to the literature, cellular uptake of particles can be affected by many factors, including particle size (Zauner et al 2001), the composition of particles, surface properties (modification, charge, etc.), cell lineage and cell density (Jung et al 2000). In these experiments, PEG modification was considered to be the key character that determines the efficiency of cellular uptake. As reported by Evangelos et al (2007), PEG modification enhanced the cellular uptake of nanoparticles, and increasing the PEG content of nanoparticles resulted in decreased cellular uptake. More PEG-40 NLCs were taken up by A549 cells compared with PEG-100 NLCs. Attachment of the particles to the cell membrane (the first step of the particle uptake process) is greatly affected by the surface charge of the particles (Lorenze et al 2006). In general, the negatively charged cell membrane has a tendency to absorb positively charged or neutral nanoparticles. The zeta potential of PEG-NLCs is close to zero (about  $-10$  mV). In contrast, the zeta potential of NLCs is  $-32.53 \pm 0.43$  mV, indicating a negative surface charge. The electronic repulsion between NLCs and A549 cells reduced absorption of NLCs to A549 cells.

### Anti-tumour effects in nude mice bearing A549 lung cancer

The anti-tumour effects of HCPT-loaded NLCs and PEG-NLCs were evaluated in-vivo using A549-bearing nude mice. Figure 8 shows the RTV in mice with time. Tumour growth was significantly inhibited in all groups except the negative control group ( $P < 0.05$ ). PEG-NLCs, especially PEG-40

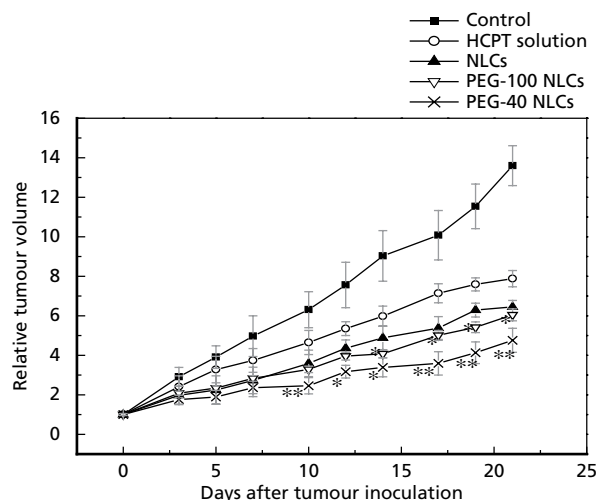


**Figure 8** Effect of treatment with HCPT injection, NLCs, PEG-40 NLCs and PEG-100 NLCs on tumour growth in mice. Control mice were given saline. Data are mean  $\pm$  s.d. ( $n = 6$ ). \* $P < 0.05$ ; \*\* $P < 0.01$  vs HCPT solution.

NLCs, had a notably enhanced anti-tumour efficacy compared with HCPT solution ( $P < 0.01$ ). This could be for several reasons. First, the HCPT injection solution used was a solution of HCPT carboxylate, whereas the HCPT encapsulated in PEG-NLCs was the active lactone form; it is therefore reasonable that better anti-tumour effect could be accomplished. Second, the sustained-release characteristic of PEG-NLCs may prolong the exposure of tumour cells to the effects of the anti-tumour drug, which is essential for S-phase-specific drugs like HCPT. Third, PEG-40 NLCs avoid uptake by the RES, and thus increase the HCPT concentration in non-RES tissues. Meanwhile, PEG-NLCs loaded with HCPT could accumulate in tumours because of the EPR effect.

### Conclusion

NLCs loaded with HCPT have been successfully modified with PEG stearate of different molecular weights. This formulation protected the active lactone form of HCPT. Both the length and the grafting density of the PEG chains influenced the in-vivo behaviour of the PEG-NLCs. PEG-NLCs, especially PEG-40 NLCs, had a longer circulation time and showed less uptake by the RES than unmodified NLCs. Interestingly, PEG-NLCs resulted in significantly enhanced uptake by the lungs after i.v. injection in mice. Cellular uptake by A549 cells was also high with PEG-NLCs. In-vivo anti-tumour experiments indicated that HCPT-loaded PEG-NLCs, especially PEG-40 NLCs, have superior efficacy against the A549 tumour. These results demonstrate that PEG-NLCs are a promising delivery system for HCPT in the treatment of lung cancer.

### References

- Alexander, V. K. (2006) Polymer genomics: An insight into pharmacology and toxicology of nanomedicines. *Adv. Drug Deliv. Rev.* **58**: 1597–1621
- Bazile, D., Prud'Homme, C., Bassoullet, M. T., Marlard, M., Spenlehauer, H., Veillard, M. (1995) Stealth MePEG-PLA nanoparticles avoid uptake by the mononuclear phagocytes system. *J. Pharm. Sci.* **84**: 493–498
- Cortesi, R., Esposito, E., Maietti, A., Menegatti, E., Nastruzzi, C. (1997) Formulation study for the antitumor drug camptothecin: liposomes, micellar solutions and a microemulsion. *Int. J. Pharm.* **308**: 183–189
- Desai, M. P., Labhasetwar, V., Walter, E., Levy, R. J., Amidon, G. L. (1997) The mechanism of uptake of biodegradable microparticles in Caco-2 cells is size dependent. *Pharm. Res.* **14**: 1568–1573
- Dziubla, T., Muzukantov, V. (2006) Nanocarriers for the vascular delivery of drugs to the lungs. In: Torchilin, V. P. (ed) *Nanoparticulates as drug carriers*. Imperial College Press, London, pp 499–526
- Evangelos, C. G., Maria, H., Evangelia, P., Konstantinos, A. (2007) Anticancer activity of cisplatin-loaded PLGA-mPEG nanoparticles on LNCaP prostate cancer cells. *Eur. J. Pharm. Biopharm.* **67**: 1–8
- Hawley, A. E., Illum, L., Davis, S. S. (1997) Preparation of biodegradable, surface engineered PLGA nanospheres with enhanced lymphatic drainage and lymph node uptake. *Pharm. Res.* **14**: 657–661
- Hu, F. Q., Jiang, S. P., Du, Y. Z., Yuan, H., Ye, Y. Q., Zeng, S. (2005) Preparation and characterization of stearic acid nanostructured

- lipid carriers by solvent diffusion method in an aqueous system. *Colloid Surface B: Biointerfaces* **45**: 167–173
- Igor, C., Jean, M. M., Ganesh, D. S., Jean, F. R., Michel, M. (1998) Kinetics of lactone hydrolysis in antitumor drugs of camptothecin series as studied by fluorescence spectroscopy. *Biochim. Biophys. Acta*. **1379**: 353–366
- Inaba, M. (1994) Kinetic analysis of cell-killing action of DNA topoisomerase I and II inhibitors, Abstract of Research Works for the General Research A of Subject Number 05302061 with a Grants-in-Aid for Scientific Research from the Ministry of Education. *Science, Sports and Culture of Japan*. 57–61
- Jaxel, C., Kohn, K. W., Wani, M. C., Wall, M. E. Pommier, Y. (1989) Structure-activity study of the actions of camptothecin derivatives on mammalian topoisomerase I: Evidence for a specific receptor site and for a relation to antitumour activity. *Cancer Res.* **49**: 1465–1469
- Jeon, S. I., Andrade, J. D. (1991) Protein-surface interactions in the presence of polyethylene oxide: II Effect of protein size. *J. Colloid Interf. Sci.* **142**: 159–166
- Jeon, S. I., Lee, J. H., Andrade, J. D., Gennes, P. G. (1991) Protein-surface interactions in the presence of polyethylene oxide: I Simplified theory. *J. Colloid Interf. Sci.* **142**: 149–158
- Jung, T., Kamm, W., Breitenbach, A., Kaiserling, E., Xiao, J. X., Kissel, T. (2000) Biodegradable nanoparticles for oral delivery of peptides: is there a role for polymers to affect mucosal uptake. *Eur. J. Pharm. Biopharm.* **50**: 147–160
- Leyang, Z., Mi, Y., Qin, W., Yuan, L., Rui, G., Xiqun, J., Changzheng, Y., Baorui, L. (2007) 10-Hydroxycamptothecin loaded nanoparticles: preparation and antitumor activity in mice. *J. Control Release* **119**: 153–162
- Lorenze, M. R., Holzapfel, V., Musyanovych, A., Nothelfer, K., Walther, P., Frank, H., Landfester, K., Schrezenmeier, H., Mailandr, V. (2006) Uptake of functionalized, fluorescent-labeled polymeric particles in different cell lines and stem cells. *Biomaterials* **27**: 2820–2828
- Maeda, H., Wu, J., Sawa, T., Matsumura, Y., Hori, K. (2000) Tumor vascular permeability and the EPR effect in macromolecular therapeutics: a review. *J. Control. Release* **65**: 271–284
- Maeda, H., Fang, J., Inutsuka, T., Kitamoto, Y. (2003) Vascular permeability enhancement in solid tumor: various factors, mechanisms involved and its implications. *Int Immunopharmacol.* **3**: 319–328
- Mi, Z., Burke, T. G. (1994) Differential interactions of camptothecin lactone and carboxylate forms with human blood components. *Biochemistry* **33**: 10325–10336
- Michalowski, C. B., Guterres, S. S., Dalla Costa, T. (2004) Microdialysis for evaluating the entrapment and release of a lipophilic drug from nanoparticles. *J. Pharmaceut. Biomed.* **35**: 1093–1100
- Moghimi, S. M., Hunter, A. C., Murray, J. C. (2001) Long-circulating and target-specific nanoparticles: theory to practice. *Pharmacol. Rev.* **53**: 283–318
- Müller, R. H., Radtke, M., Wissing, S. A. (2002) Solid lipid nanoparticles (SLN) and nanostructured lipid carriers (NLCs) in cosmetic and dermatological preparations. *Adv. Drug Deliv. Rev.* **54** (Suppl. 1): S131–S155
- O'Leary, J., Muggia, F. M. (1998) Camptothecins: a review of their development and schedules of administration. *Eur. J. Cancer* **34**: 1500–1508
- O'Reilly, S. O., Rowinsky, E. K., Slichenmyer, W., Donehower, R. C., Forastiere, A. A., Ettinger, D. S., Chen, T. L., Sartorius, S., Grochow, L. B. (1996) Phase I and pharmacologic study of topotecan in patients with impaired renal function. *J. Clin. Oncol.* **14**: 3062–3073
- Peracchia, M. T., Vauthier, C., Passirani, C., Couvreur, P., Labrre, D. (1997) Complement consumption by poly(ethylene glycol) in different conformations chemically coupled to poly(isobutyl 2-cyanoacrylate) nanoparticles. *Life Sci.* **61**: 749–761
- Qingyu, X., Minting, W., Fu, C., Tao, G., Yanlin, J., Zhirong, Z., Yuan, H. (2007) Lung-targeting delivery of dexamethasone acetate loaded solid lipid nanoparticles. *Arch. Pharm. Res.* **40**: 519–525
- Sadzuka, Y., Hirota, S. (1997) Physical properties and tissue distribution of adriamycin encapsulated in polyethyleneglycol-coated liposomes. *Adv. Drug Deliv. Rev.* **24**: 257–263
- Serrano, A. G., Perez-Gil, J. (2006) Protein-lipid interactions and surface activity in the pulmonary surfactant system. *Chem. Phys. Lipids.* **141**: 105–118
- Shimada, K., Miyagishima, A., Sadzuka, Y., Nozawa, Y., Mochizuki, Y., Ohshima, H., Hirota, S. (1995) Determination of the thickness of the fixed aqueous layer around polyethyleneglycol-coated liposomes. *J. Drug Target.* **3**: 283–289
- Sims, G.E., Snape, T. J. (1980) A method for the estimation of polyethylene glycol in plasma protein fractions. *Anal. Biochem.* **107**: 60–63
- Wani, M. C., Ronman, P. E., Lindley, J. T., Wall, M. E. (1980) Plant antitumor agents. 18. Synthesis and biological activity of camptothecin analogues. *J. Med. Chem.* **3**: 554–560
- Williams, J., Lansdown, R., Sweitzer, R., Romanowski, M., LaBell, R., Ramaswami, R., Unger, E. (2003) Nanoparticle drug delivery system for intravenous delivery of topoisomerase inhibitors. *J Control Release* **91**: 167–172
- Yasuyuki, S., Akiko, N., Rieko, H., Atsuo, M., Yasuo, N., Sadao, H., Takashi, S. (2002) Effects of mixed polyethyleneglycol modification on fixed aqueous layer thickness and antitumor activity of doxorubicin containing liposome. *Int. J. Pharm.* **238**: 171–180
- Zauner, W., Farrow, N. A., Hainess, A. M. R. (2001) In vitro uptake of polystyrene microspheres: effect of particle size, cell line and cell density. *J. Control. Release* **71**: 39–51
- Zerrin, S., Nilufer, Y., Tamer, B. (2006) Preparation and characterization of polymeric micelles for solubilization of poorly soluble anticancer drugs. *Eur. J. Pharm. Biopharm.* **64**: 261–268
- Zhou, J., Fan, Y. J., Chen, D. N., Liang, Z., Yang, W. L. (1991) An experimental evaluation of the antitumor activity and toxicity of camptothecin versus 10-hydroxycamptothecin. *Chin. J. Cancer.* **10**: 198–202